Pollution 2022, 8(2): 355-372
DOI: 10.22059/POLL.2021.321164.1049

RESEARCH PAPER

High Content of Sulfur in Liquid Stream Removal via new Carbonous Nano Adsorbent: Equilibrium, Kinetic study

Seyyed Salar Meshkat[1,*], Zeinab Hosseini Dastgerdi[1], Vahid Abkhiz[2] and Asieh Hagh Shenas[1]

1. Faculty of Chemical Engineering, Urmia University of Technology, P.O.Box 5716617165, Urmia, Iran
2. Pars Oil & Gas Company (POGC), P.O.Box 14147 13111, Tehran, Iran

Received: 28.03.2021, Revised: 16.11.2021, Accepted: 21.11.2021

ABSTRACT
This research evaluates dibenzothiophene (DBT) adsorptive removal from the liquid stream on the graphitic carbon nitride (GCN) as a synthesized adsorbent at 25 ^{0}C with 3 g for 600 min. The morphological properties of GCN have been investigated by Brunauer–Emmett–Teller (BET), Transmission Electron Microscopy (TEM), Scanning Electron Microscopy (SEM), and X-ray Diffraction (XRD). The study of the characteristic properties of nano adsorbent proves the suitability of the synthesized GCN in mercaptan adsorption process with the obtained data showing a good agreement with Freundlich model. The equilibrium capacity of DBT adsorption has been calculated at about 39.1 mg/g. This has also been 25.8 mg/g for TBM (tertiary butyl mercaptan). The adsorption capacity has increased by adding to the adsorbent dosage. Thermodynamic studies expose the negative values for ΔS^0 (-8.99 kJ/mol. K), ΔH^0 (-21.05 kJ/mol), and ΔG^0 (8.91 kJ/mol), which demonstrate that DBT adsorption has been a natural exothermic process. In addition, this experiment verifies that the substitution of N into the carbon structure improves the DBT removal efficiency in comparison with pristine CNT as an adsorbent. The removal efficiency of DBT onto GCN has been approximately 80%, i.e. 20% higher than that of pure CNT. Results show that the adsorption capacity of DBT as a cyclic source of mercaptan has been higher than Tertiary butyl mercaptan (TBM) as a liner one. The DBT adsorption mechanism is done by π–π electron interactions between the aromatic structures of DBT, lone-pair electrons of the S atoms, and the pyridinic GCN planes band.
Keywords: nanostructure; adsorption; carbon nitride; dibenzo thiophene; equilibrium

INTRODUCTION

In recent decades due to the harmful effects of the emission of sulfur components from fossil fuels on the environment, sulfur removal from gas liquids and refinery products such as gasoline has been considered. Due to the crucial environmental effects of the mercaptans such as acid rain and catalyst poisoning which are formed by combustion of the fuel, the content of sulfur is to restricted 15 and 30 ppm for diesel and gasoline by the environmental regulations (Khan et al. 2013; Hoseini & Meshkat, 2019; Fallah & Azizian, 2012). Mercaptans are one of the major contributors to fossil fuels and nowadays, the removal of thiophenic compounds in the flow of gas liquids and refinery wastewater has become a very important issue all over the world (Fallah & Azizian, 2012). Due to the environmental regulations around the world, governments have recently set strict regulations to reduce the amount of sulfur in fuel, one of its main focuses being to reduce the sulfur content of fuels used by vehicles. According to government regulations, permissible sulfur content is reported to be acceptable from 0.1% to 0.5% by weight sulfur compounds (Advances & Srivastava, 2012).

Much attention has been devoted to investigate and apply different techniques to remove

* Corresponding author Email: s.meshkat@che.uut.ac.ir

sulfur compounds from fluid hydrocarbon streams (Deliyanni et al, 2009; Kumagai etal., 2010). Various methods have been evaluated such as hydrodesulfurization (HDS), extractive desulfurization, bio desulfurization, oxidation, and adsorption for desulfurization (Meshkat et al., 2018; Seredych & Bandosz, 2010). The scientists have completed many widespread efforts to find an inexpensive, appropriate, and notable method to substitute for hydrodesulfurization (HDS). However, HDS needs high hydrogen pressure at high temperatures and high amounts of expensive hydrogen gas are consumed by this method. Copper doped silica was set by Peng et al. to eliminate low concentration of CH_3SH where it was initiated that surface groups of CuO nanoparticles and Si-O-Cu group are more effective in adsorption of CH_3SH (Kim et al., 2006; Peng, 2019). It is reported that the MOF-199 had the highest adsorption capacity for dimethyl sulfide (i.e., 8.48 g S/100 g sorbent). The adsorption method is suitable for sulfur removal due to operating conditions, low cost, and non-contamination in the environment, which is used in many applications to remove contaminants. Also, the advantage of this method is the ability to control the process under the influence of the type of adsorption material, the properties of the absorbing material, and material are in the contaminated environment (Saleh et.al. 2018). Adsorption technology recently has been developed by acquiring adsorbents with high adsorption capacity, the possibility of regeneration and reusability, and selective adsorption of materials for desulfurization. Since the last decade, considerable attention has been paid to the modification of adsorbents in order to develop the adsorption capacity. In this regard, a great deal of research on the modification of the carbon-based adsorbents has been done with high porosity and high surface area materials such as carbon nanotubes, activated carbon, graphene and etc. (Moosavi et al., 2012; Yua et al., 2013; Muzica et al., 2015). Consequently, novel nano adsorbents that are low-cost and facile synthesized are still highly essential to be established as adsorbents for the mercaptan removal from the liquid stream.

Due to the unique structure and semiconductor properties, graphitic carbon nitride (g-C_3N_4) is one of the various two-dimensional layered materials, which was used as photocatalysts in wastewater purification and environmental treatment methods (Zheng et al., 2015; Thomas et al., 2008). Within the literature review, only a little study has performed on the application of g-C_3N_4 for mercaptan removal. g-C_3N_4 as well as its derivatives have seemed as metal-free adsorbents due to their useful properties such as non-toxicity, stability, reusability, and easy preparation has been studied (Zhao et al., 2019). Due to the six-nitrogen lone-pair electrons, the negatively charged functionalities are formed in highly ordered tri-s-triazine units of g-C_3N_4 (Muzic et al., 2008; Cao et al., 2015; Cai et al., 2017). Research has reported that carbon nitride graphics have been used in aqueous solutions due to their reusability and chemical stability to absorb heavy metal ions and organic pollutants (Hu et al., 2015). Furthermore, the amino groups on the surface of g-C_3N_4 are also active in removing mercaptan. Various studies have been reported to enhance the metal adsorption capacity of carbon nitride graphics, such as metal oxide by Gao & et.al by clothing functional polymer method (Gao et al., 2016).

In this paper, we synthesized a simple, inexpensive, efficient, and environmentally friendly method to fabricate the porous g-C_3N_4 (GCN) with modified porosity and surface area to improve the adsorbent properties in the dibenzothiophene (DBT) as a cyclic basis of mercaptan and tertiary butyl mercaptan (TBM) as a liner mercaptan source adsorption process. SEM, XRD, TEM, BET is employed to characterize the morphology and structure of the synthesized adsorbent. The adsorption mechanism and kinetic and isotherm were also studied by suitable models.

MATERIALS AND METHODS

Melamine (99%), potassium hydroxide (98%), hydrochloric acid (>98%), were all purchased from Merck Company. Dibenzothiophene (DBT) (99%), tertiary butyl mercaptan (TBM) (99%) were got from Aldrich Company.

In order to synthesize the bulk g-C_3N_4 (GCN), 5 g of melamine was placed in a boat and placed in a furnace at 550 ºC for 2 h in static air with a heating rate of 5 ºC /min. After that, 0.1 g of bulk GCN was mixed with 0.2 g of KOH and 5 mL of H_2O and sonicated for 3 min. the water was evaporated at 100 ºC in an oven to get the powder. The powder was annealed at 350 ºC for 1.5 hours in air current (P=1bar) with a heating rate of 5 ºC /min in a tubular furnace. The yellow powder was cooled down and was washed with dilute HCl (5 wt.%) and then with H_2O until pH = 7.

Parallel batch experiments were carried out to evaluate the mercaptan adsorption from the liquid stream of the model fuel. For this end, 0.5 g of the prepared adsorbent (GCN) was added to 100 ml of the flask of the model fluid solution containing 1000 ppm of DBT. The adsorbent was then sieved, and the residual mercaptan concentration in the model fluid was obtained by total Sulfur analysis instrument (TS-100) with a detection limit of 0.5 ppm which had an uncertainty of less than ±5%. DBT adsorption process parameters such as mass loaded adsorbent (g), temperature (^{0}C), time (min) and DBT concentration (ppm) were varied 0.1-3g, 20- 60 ^{0}C, 10- 1440 min and 50 -2000 ppm, respectively. These parameters were optimized by the design of expert software response surface methodology software (RSM-DOE). In this work we do our design of experiment optimization by four parameters: input concentration (X_1: C_0, PPM), adsorbent mass (X_2: mC_3, g), time (X_3: t, min), temperature (X_4: T, °C), Box-Behnken design (BBD) with 5 centre points. The capacity of the synthesized adsorbent (mg/g) was considered from Eq. (1):

$$q_e = \frac{C_i - C_e}{m} V \quad (1)$$

Which q_e implies the adsorption process capacity (mg/g), C_i and C_e are the initial mercaptan concentration and equilibrium concentration (ppm), m indicates the adsorbent mass loaded (g) and V is solution volume (L).

The evaluation of adsorption kinetics study was done at 25 °C for the dibenzothiophene (DBT) as a mercaptan source with the initial concentration of 1000 mg/ L at various times from 5 min to 1440 min. The kinetic study was considered using three models (Jha et al., 2019; Mguni et al., 2018; Xu et al., 2013): pseudo-first-order model, pseudo-second-order model, and intraparticle model, described by the following equations.

This model assumes that the adsorption rate of the sample is directly proportional to the difference in saturation concentration of the adsorbed molecule on the adsorbent surface and the amount of adsorbent at different times Pseudo-first-order model is followed by Eq. (2):

$$\frac{dq_t}{dt} = k_1(q_e - q_t), \quad (2)$$

where q_e and q_t respectively are the amount of absorbed material by an adsorbent at time of equilibrium and time (t) in (mg / g), and k_1 is the first-order pseudo constant in (1/min). By integrating this equation and assuming boundary conditions, t = t, q = 0, q = q_t, t = 0, the form of the equation is expressed as the following Eq. (3):

$$log\ log\ (q_e - q_t) = log\ log\ q_e - \frac{k_1}{2.303}\ t. \quad (3)$$

Pseudo-second-order model constants are discovered from Eq. (4):

$$\frac{dq_t}{dt} = k_2 \left(q_e\_ q_t\right)^2. \quad (4)$$

That k_2 is the constant pseudo-second-order constant. By integrating the equation and applying boundary conditions q = 0, t = 0 and q = q_t, t = t, the linear form of the equation is obtained as follows Eq. (5):

$$\frac{t}{q_t} = \frac{1}{k_2 q_e^2} + \frac{1}{q_e} t. \quad (5)$$

Weber and Morris have announced the intraparticle diffusion model to distinguish the mass transfer resistance of the adsorption process onto the adsorbent are given by Eq. (6):

$$q_t = k_i.t^{0.5} + C, \quad (6)$$

where, C demonstrates the width of the boundary layer and k_i is the intraparticle diffusion rate constant (mg/g. $(min)^{0.5}$) respectively. The constant C and k_i are computed by the plot of q versus $t^{0.5}$ (Tang et al., 2018; Earvin et al., 2017; Habimana et al., 2016. In this study, from different isotherms, Langmuir, Freundlich, and Dubinin–Radushkevich (D-R) are selected for discussion for the adsorption data and the best-fitted one was chosen for the isotherm evaluation. Langmuir absorption assumes that the absorbent only interacts with a limited number of uniformly adsorbed sites, and that absorption is limited to only one single layer on the surface. The mathematical relation of this model is in Eq. (7):

$$q_{eq} = \frac{K_L C_{eq}}{1 + k_L C_{eq}}, \quad (7)$$

Where q_{eq} is the equilibrium adsorption capacity and q_{max} is the maximum absorption capacity, both in (mg/g), C_e is the concentration of soluble species at the instant of equilibrium in (mg/L) and K_L is Langmuir constant. The linear relationship of Eq. 8 is expressed in the following form Eq. (8):.

$$\frac{c_e}{q_e} = \frac{1}{q_{max} k_L} + \frac{c_e}{q_{max}} \quad , \quad (8)$$

By plotting the C_{eq} / q_{eq} diagram in terms of C_e, q_{max} values of the slope of the graph and K_L are obtained. The adaptation of obtained data with Langmuir isotherm expresses the uniform nature of the adsorbent surface that describes the formation of a single-layer coating of an absorbing molecule on the absorber surface.

The Langmuir isotherm's basic characteristic is a dimensionless constant (R_L) that is used to represent the efficiency of the absorption process and is calculated according to Eq.9 Where C_0 is the highest initial concentration of adsorbed material in (mg/L). If R_L is zero, the absorption system is irreversible and if the RL is between zero and one, it is desirable and if it is equal to 1, it is undesirable (Tang et al., 2013; Batten et al., 2018).

$$R_L = \frac{1}{1 + k_L C_0} \quad , \quad (9)$$

The experimental relationship of Freundlich based on the absorption of multilayers on heterogeneous surfaces that main relationship and its linear form are shown in the following relationships, respectively Eqs. (10 &11): (Tang et al., 2013; Batten et al., 2018)

$$q_{eq} = k_f C_{eq}^{\frac{1}{n}} , \quad (10)$$

$$In(q_{eq}) = \frac{1}{n_F} In(C_{eq}) + In(K_F) . \quad (11)$$

The parameters n_F and K_f are constants of temperature and absorption and adsorbent properties, respectively, that express capacity and intensity of adsorption. From the plot of ln q_{eq} curve in terms of ln Ce, lnK_f counted which represents absorption capacity, and 1/n of the line slope, which indicates absorption rate.

Evaluation of the structure and size of the synthesized adsorbent is performed by Transmission Electron Microscopy (TEM) images which are taken by JEOL 1200 EXI instrument. Scanning electron microscopy (SEM; Mira 3-XMU model with accelerating potential 7.0 kV) was used to study the morphology of the prepared nanocomposites. The evaluation of the thermal stability of the synthesized adsorbents was accomplished by use of thermogravimetric analysis (TGA) which was utilized by a PL thermal analyzer (Polymer Laboratories, TGA 1000 and Shropshire, UK). It is used to prove the thermal stability and discuss the decomposition pattern of the prepared adsorbent. TGA analysis data were performed under an N_2 atmosphere with a 50 mL/min flow rate and heating rate of 10 °C/min. To demonstrate the formation of the adsorbent X-ray diffraction (XRD) patterns were carried out with a Philips diffractometer (PW- 1730) (Lump Cu-kα, λ=1.54 Å). The calculation of surface area and porous characterization were performed by N_2 adsorption/desorption at 77 K utilization of an ASAP-2010 porosimeter (Micromeritics Corporation GA) with Brunauer–Emmett–Teller (BET) isotherm. To attain information about the elemental composition of the synthesized adsorbent, the Elemental analysis was approved by the Costech device, ECS4010 model in which the samples were heated at 1000 °C.

RESULTS AND DISCUSSION

The crystallinity of the synthesized porous carbon nitride as an adsorbent was premeditated by XRD patterns which were shown in Fig.1. As Fig. 1 shows, the strong peaks at 2θ of 29.2° is the characteristic g-C_3N_4 (GCN) peaks. It reflects the characteristic interlayer stacking in the conjugated aromatic systems, is famous as the (002) peak of the graphitic materials. A weak peak at 15.1° named to the (100) peak is associated with the in plane repeating structural themes of the conjugated aromatic systems. It can be resolved that GCN owns single or few layers (Lin et al., 2012; Sano et al., 2005; JabariSeresht et al., 2013).

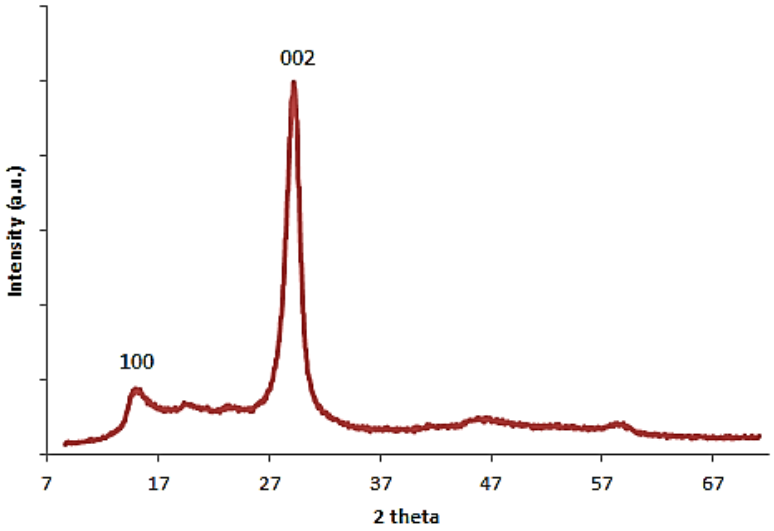

Fig 1. XRD pattern of the synthesized adsorbent

The TEM image of the synthesized nanostructure adsorbents displayed in Figure. 2. The structure was highly porous, and it designated the nanometric structure of the g-C_3N_4 sheets with high porous sheets. The SEM images of g-C_3N4 are presented in Figure. 3. This figure displays the high porosity of the adsorbent structure with a small pore size.

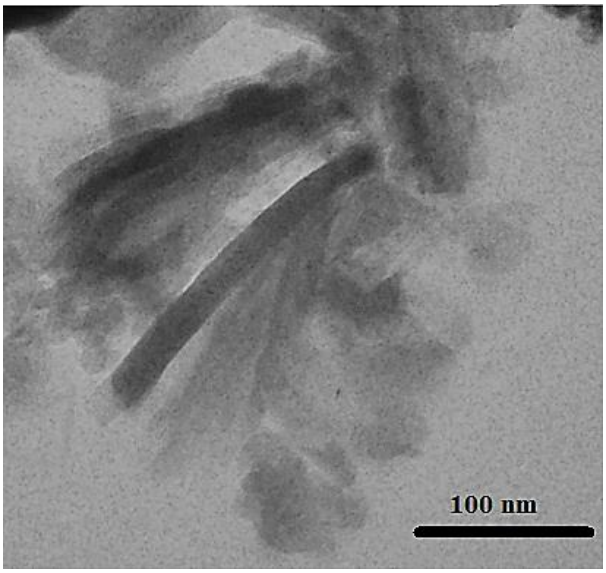

Fig 2. TEM image of the synthesized adsorbent

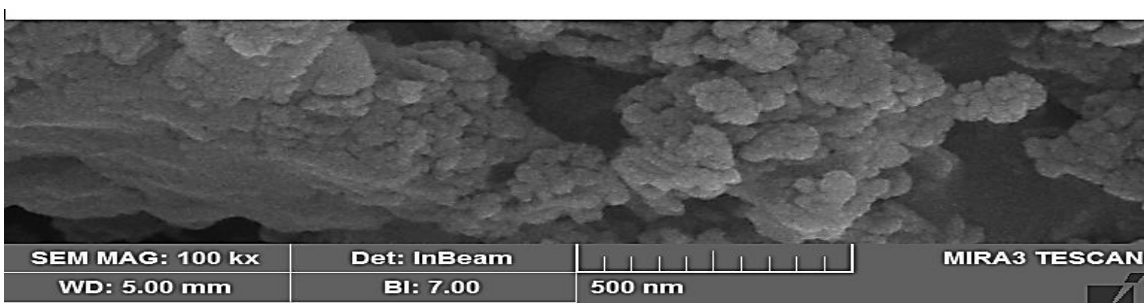

Fig 3. SEM image of the synthesized g-C_3N_4

The N_2 adsorption/desorption isotherm of the synthesized GCN is demonstrated in Figure. 4 Nitrogen adsorption/desorption was achieved with the utilization of liquid nitrogen at 77 K. The BET adsorption isotherms fitting line in the relative pressure (P/P_0) range of 0.2–0.35 was drawn to calculate the GCN specific surface area. The total pore volume is attained by the amount of liquid nitrogen adsorbed at the relative pressure of 0.98 atm. The average pore diameter (D_p) was considered with the aid of the resulting equation: $D_p = 4V_T/S$ (Díaz-Díez et al., 2005), where V_T is the total volume of pores, and S is the BET surface area. As shown in Figure. 5, a typical Ⅳ type curve and a hysteresis loop at the relative pressures of 0.4–0.98 atm. The results have emphasized the presence of slit-shaped pores between layers of g-C_3N_4 (Szabo et al., 2005). The results of the synthesized adsorbents present, the main pore size fits a mesoporous material and verified the nano porous category for the synthesized g-C_3N_4. In addition, the total pore volume of the g-C_3N_4 was 0784 cm^3/g at P/P_0 of 0.98. The summary of the g-C_3N_4 BET surface area, pore size, and pore volume calculation are revealed in Table 1.

Table 1. Physical properties of the synthesized adsorbent.

Samples	S_{BET} [m^2/g]	Total pore volume [cm^3/g]	Mean pore diameter [nm]
g-C_3N_4	432.4	0.784	31.179

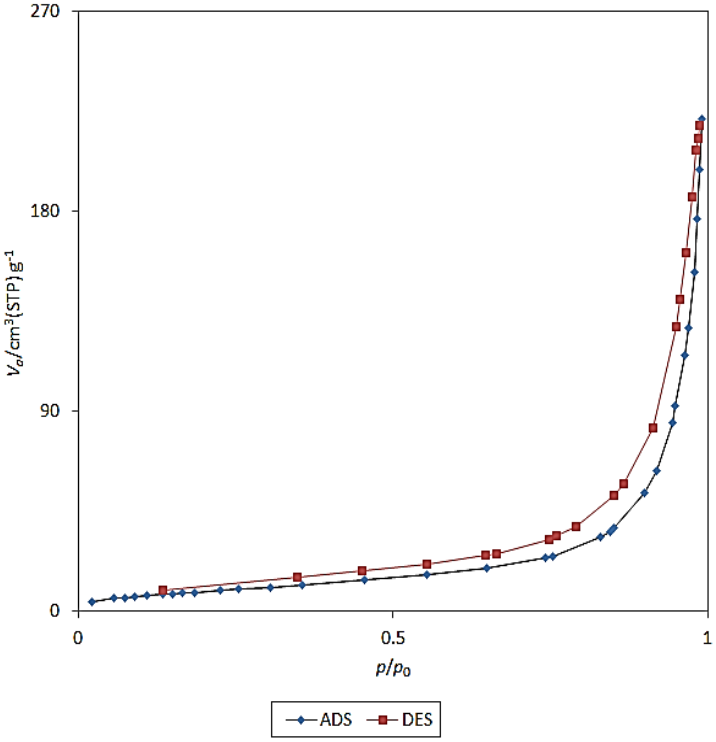

Fig 4. Nitrogen adsorption/desorption isotherms of g-C_3N_4

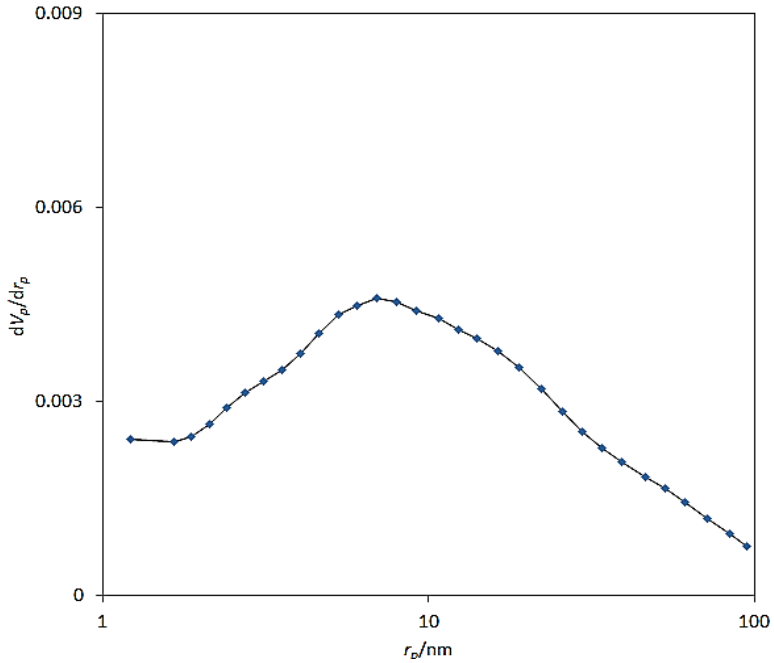

Fig 5. Pore sized distribution of g-C_3N_4.

The effect of the synthesized adsorbent mass loading on DBT removal was studied by use of different amounts of the adsorbent. In this section, the mercaptan initial concentration, temperature, and time were set in 100 ppm, 25 ^{0}C, 10 h, respectively. The maximum removal efficiency of about 80% was reached at 3 g, as shown in Figure. 6. The porous textures and surface chemical properties of the synthesized adsorbent increased the mercaptan adsorption on the GCN as an adsorbent. It is concluded from the results of this experiment that the surface chemical properties largely exaggerated the specific surface area or pore volume in g-C_3N_4 defining the adsorption capability. In addition, the surface N atoms improved the capacity of DBT adsorption by making available a high surface area and many adsorption sites for mercaptan removal on the adsorbent surface and providing C–N bonds over the sorbent surface. Also, the DBT adsorption mechanism is done by π–π electron donor-acceptor interactions between the aromatic structures of DBT and the lone-pair electrons of the mercaptan S atoms and the pyridinic g-C_3N_4 planes band. In comparison (Figure.6), the removal efficiency of the DBT adsorption on the GCN is much improved via the surface modification than the pristine carbon nanotube (CNT).

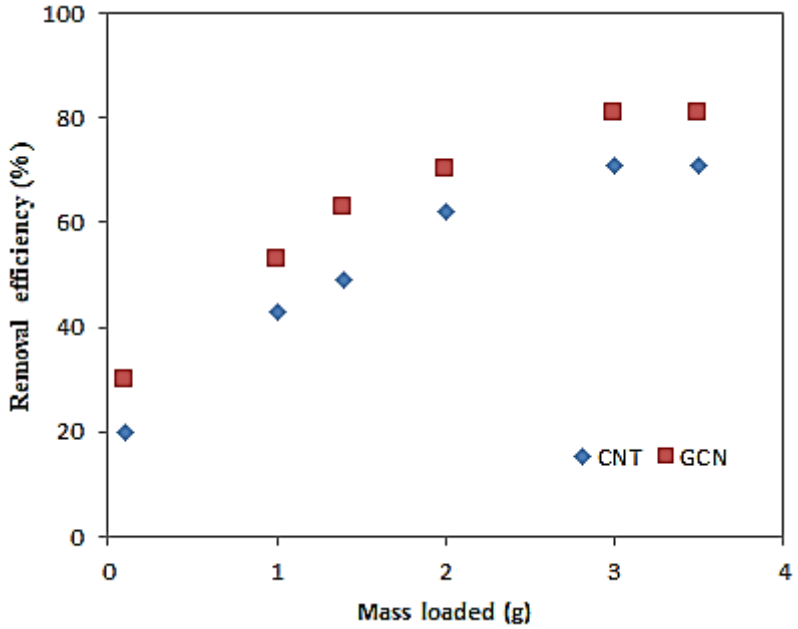

Fig 6: Effect of mass loaded on the DBT adsorption onto the GCN vs. CNT

The kinetic study was carried out at various times and 25 ^{0}C, 3 g mass-loaded, and 1500 ppm of DBT initial concentration. The necessary equilibrium time for mercaptan adsorption on GCN as an adsorbent was considered in several contact times. As concluded from Figure. 7, the optimum amount of contact time is about 10 h (600 min). DBT molecules reached and enclosed the adsorbent pores. This equilibrium time attained about 600 min, that the DBT removal efficiency of the adsorbent reduced after the equilibrium time. The adsorbent's maximum equilibrium capacity was about 39.1 mg/g at 600 min. To control the removal efficiency and mass transfer resistance, a kinetic study was performed. The kinetic study data were fitted by 2 kinetic models, pseudo-first-order and pseudo-second-order. It is concluded from Table 2 and Figure. 8 due to the high regression coefficient the appropriate kinetic model for DBT adsorption by GCN as an adsorbent was the pseudo-second-order model. The calculated adsorption capacity exposed that it was close to the experimental one (Zhao et.al. 2008).

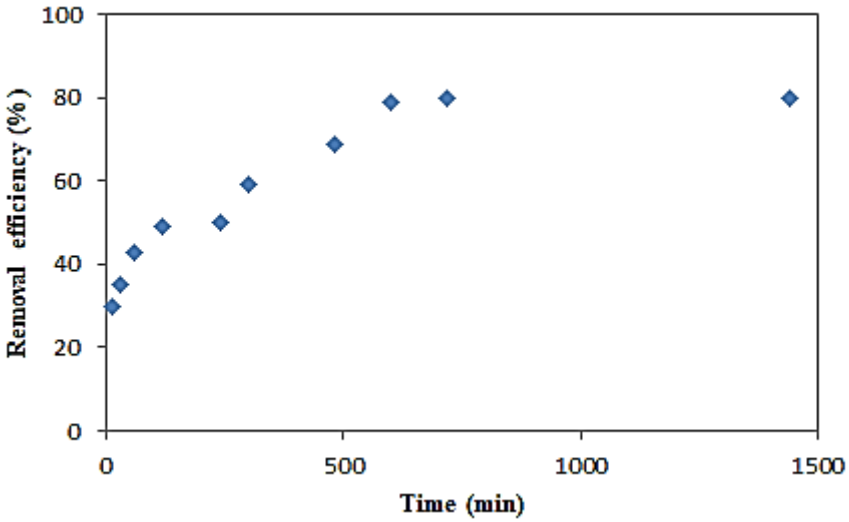

Fig 7. Effect of time on the DBT adsorption onto the GCN

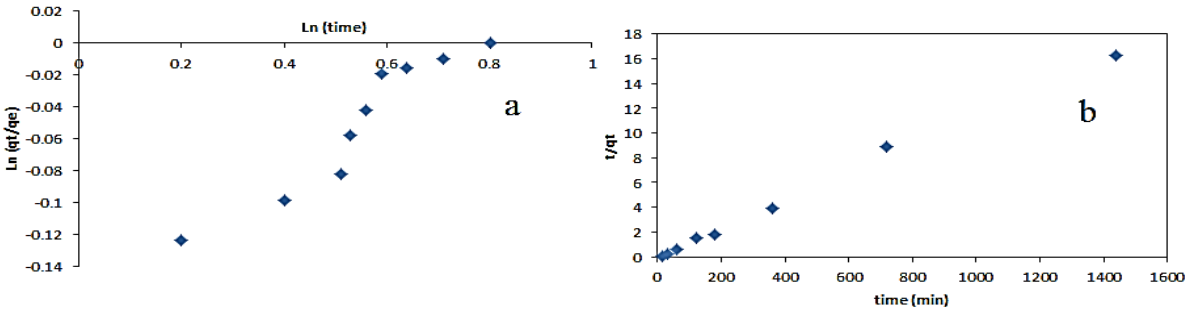

Fig 8. Kinetic study of DBT adsorption onto the GCN, a) Pseudo first order b) Pseudo second order

Table2. Kinetic adsorption parameters of DBT by GCN

	Pseudo first order			**Pseudo second order**		
q_e(experimental) (mg/g)	q_e (mg/g)	k_1(mg/g.min)	R^2	q_e (mg/g)	k_2(mg/g.min)	R^2
39.1	48.8	$7.23*10^{-2}$	0.69	38.2	$5.4*10^{-2}$	0.99

The experimental tests of the initial concentration study were done at 25 ^{0}C for 10 h contact time with 3 g of adsorbent. The results were plotted in Figure. 9 which indicated that mercaptan removal efficiency is improved by raising the initial concentration of DBT due to the enhancement of mass transfer driving force. It can be concluded from Figure. 9 that, the maximum removal efficiency of mercaptan occurred in 1500 ppm. The maximum removal efficiency of the DBT adsorption is about 80%. It is obvious that the removal efficiency was reduced via the decrease of initial concentration, which is described by the fact that at high DBT concentrations the sites of the adsorbent are occupied by adsorbate molecules and there are not enough active sites to accommodate the mercaptan molecules and the little sites persisted.

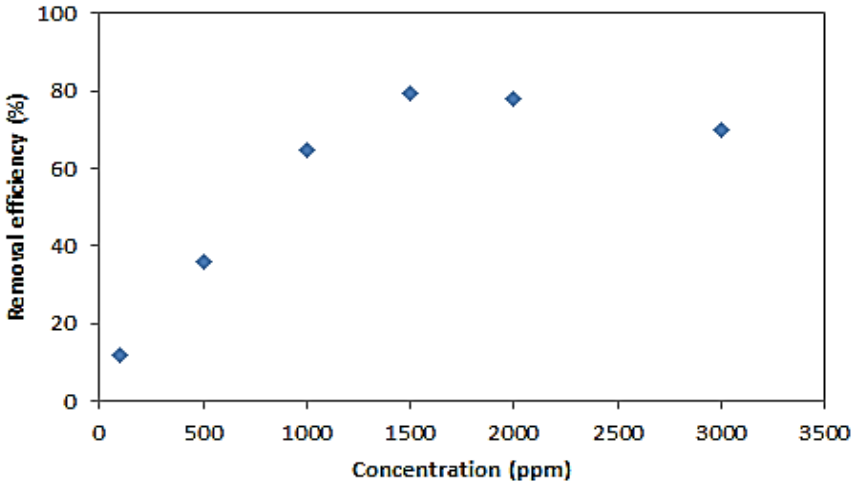

Fig 9. Effect of concentration on the DBT adsorption

As the equilibrium data were shown in Figure. 10, it was determined that the equilibrium capacity of the adsorption was about 39.1 mg/g. The equilibrium data fitting (Table 3) on the adsorption isotherms for DBT removal exposed that the Freundlich model was more appropriate than the other models. The favorable adsorption on carbonaceous adsorbents can be attained from the Figure. 10 and summarized data in Table 3. The reversibility in the adsorption process and the formation of multilayer adsorption were the Freundlich isotherm

assumption, which they can be fixed well by the experiment in the considered concentration variety. Also, the Freundlich coefficient (n) is higher than 1 proved that the adsorption runs as a physisorption process, not chemisorption. For further analysis of DBT adsorption onto GCN nanostructure, Tempkin constant and the regression coefficients were presented in Table 3. It is determined from the high values of regression coefficients of the Tempkin model that the Tempkin model accomplished a better fitting than the Langmuir model for the investigation of DBT adsorption on g-C_3N_4 as an adsorbent mainly.

Table 3. Results obtained for parameters of isotherm models

	Langmuir			**Freundlich**			**Tempkin**		
Sample/parameters	b	Q_0	R^2	k_f	n	R^2	A_T	B	R^2
GCN	0.008	97.4	0.64	1.25	1.1	0.99	0.043	68.2	0.94

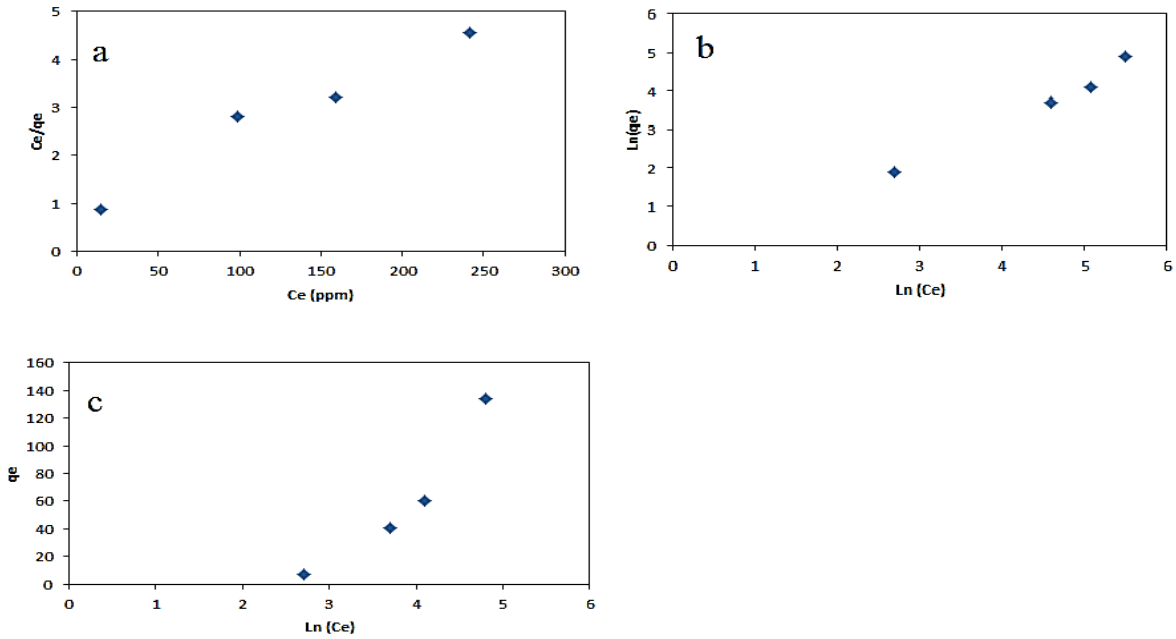

Fig 10. Isotherm study of the DBT adsorption onto the synthesized adsorbent
a) Langmuir b) Freundlich c) Tempkin

In order to evaluate the temperature effect on the DBT adsorption process on GCN as an adsorbent, the experiment was done at 25 ^{0}C for 10 h contact time with 3 g of adsorbent at various temperatures. It can be gained from Figure. 11 that due to the exothermic adsorption process, the removal efficiency of DBT (Table. 4) declines by growing the temperature. The thermodynamic parameters such as Gibbs free energy (ΔG^0), adsorption enthalpy (ΔH^0), and standard entropy (ΔS^0) were calculated from the Gibbs and vant Hoff equations announced in Eqs. (12) to (13) (Zhao et.al. 2008).

$$\Delta G^0 = -RTLn\, K_l\,, \tag{12}$$

$$Ln\,(K_l) = -\frac{\Delta H^0}{RT} + \frac{\Delta S^0}{R}\quad, \tag{13}$$

where R plays as the universal ideal gas constant (R=8.314 J/ mol. K), T stands the

temperature (K), and K_L remains the constant of Langmuir equilibrium which should be multiplied by the molecular weight of the adsorbate and by 1000 to transform the equilibrium Langmuir constant in L/mol.

By calculation the slope and intercepts of Eqs. (12) and (13) (Figure.12), the thermodynamic parameters of ΔH^0 and ΔS^0 were calculated in different temperatures. They were summarized in Table 5. The value of these parameters became −21.05 and –8.99 J/mol. K, respectively. The negative amount of ΔH^0 reveals the exothermic process of DBT removal by GCN.

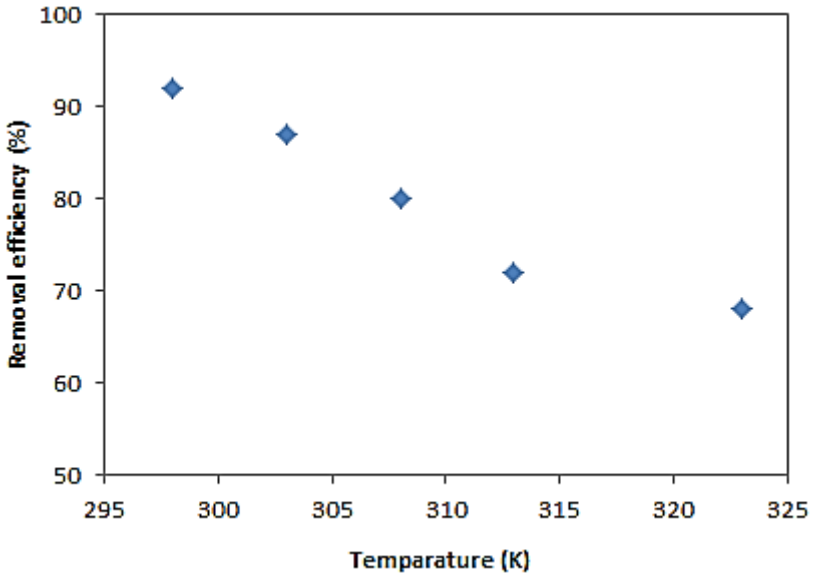

Fig 11. Effect of temperature on the DBT adsorption onto the GCN

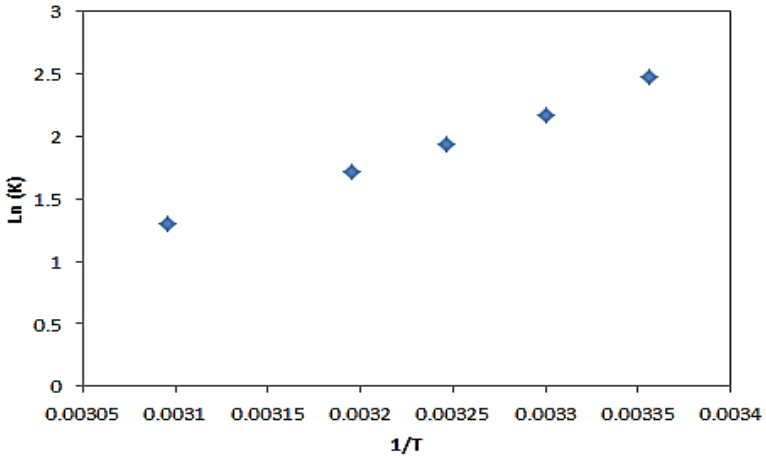

Fig 12. Thermodynamic parameters of DBT adsorption

Table 4. Effect of temperature on the adsorption of DBT

Temperature (^{0}K)	Removal efficiency (%)
298	92.1
303	87.3
313	72.2
323	67.6

Table 5. Thermodynamic parameters for DBT adsorption

Temperature (^{0}K)	ΔG^0 (KJ/mol)	ΔH^0 (kJ/mol)	ΔS^0 (kJ/mol. K)
298	8.91	-21.05	-8.99
303	10.24		
313	12.45		
323	13.47		

To study the effect of mercaptan chemical structure on the removal efficiency of synthesized adsorbent the experiment was performed at 25 ^{0}C, 1500 ppm initial concentration of mercaptan for 10 h contact time at different amounts of adsorbent mass loaded. Also, DBT was used as a cyclic mercaptan source and tertiary butyl mercaptan (TBM) was used as a non-cyclic mercaptan source. The results of this batch experiment for DBT and Tertiary Butyl Mercaptan (TBM) were plotted in Figure. 13. It is obvious that adsorbent equilibrium capacity was 39.1 and 25.8 mg/g for DBT and TBM respectively. Due to the increase of adsorbent loading, the removal efficiency value was enhanced because of the increase of active sites of adsorption. The adsorption capacity was controlled by the interaction between the g-C_3N_4 as an adsorbent and sulfur molecules. The adsorption of TBM as a liner sulfur molecule was controlled by Van der Waals interactions and Lewis base theory (Kwon et al., 2009). As nitrogen atoms in the adsorbent structure play the role as the electron-rich donor elements versus the sulfur atom in the mercaptan molecule is considered as a strong Lewis acid role. It is determined from the results that the main mechanism of the sulfur adsorption can be explained by interactions with the pair of electrons which are stated as electron-rich donor sites.

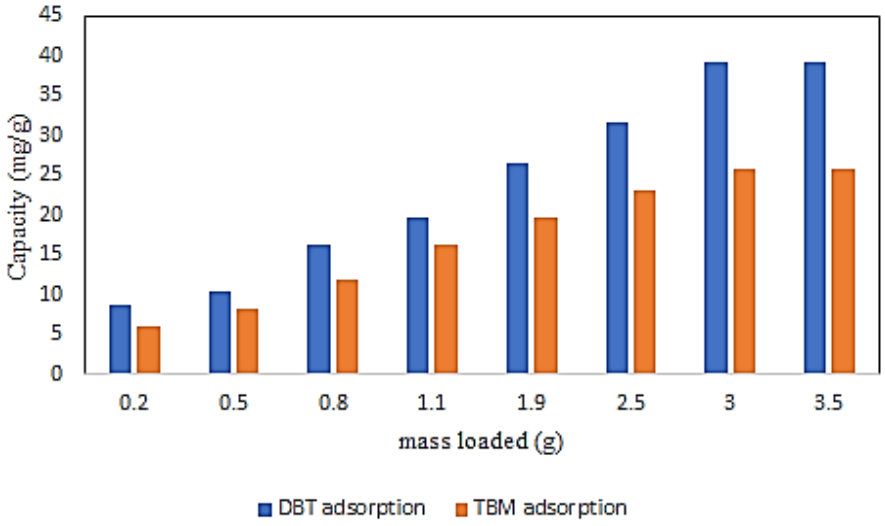

Fig 13. The comparison of adsorbent capacity in DBT and TBM adsorption vs. mass loaded

As deliberated earlier, the engagement in adsorbent pores with van der Waals bond was controlled the TBM molecules adsorption mechanism on GCN. Because of the weak authorization of the van der Waals bond in TBM adsorption, the adsorbent capacity is lower than the DBT molecules π-π interaction with GCN. The comparison in this experiment presented that the DBT adsorption capacity improved better than the TBM molecules in a linear structure which clarified by the engagement of S heterocyclic molecules in DBT π–π coupling interactions with the GCN π-electron regions (Kwon et al., 2009).

The statistical analysis of experimental data was investigated by means of Design of Expert software. The levels of factors were gained and the second order polynomial model equations (14a) in coded form, and equations (14b) with actual values, were developed to describe relations of output sulfur concentration (Y_C, C) to the four process parameters: input sulfur concentration, adsorbent loaded mass, temperature and time. Also, the validation of the models and the model coefficients was performed utilization of adsorption test results.

$$Y_C = 23.4 + 4.901X_1 - 1.8X_2 - 0.57X_3 - 0.015X_4 - 0.01X_1^{\,2} + 0.73X_2^{\,2} - 0.019X_3^{\,2} + 0.978X_4^{\,2} - 0.082X_1X_2\,, \quad (14a)$$

$$Y_q = 0.098 + 0.056X_1 - 0.011X_2 + 0.0095X_3 + 3.167*10^{-4}X_4 + + 0.002X_1^{\,2} + 0.0012X_2^{\,2} + 0.0018X_3^{\,2} - 0.019X_4^{\,2} - 0.039X_1X_2\,, \quad (14b)$$

The model's confirmation is done significantly by calculation of F-values which is 542.56. The noise may cause models F-values is only about 0.01%. The P-values lower then 0.0500 show that in the case of the concentration of sulfur response model terms X_1, X_2, X_3 and X_4^2 are significant (Table 6).

Table 6. ANOVA

source	SS	DF	F-Value	P-value
X_1	323.42	1	3371.89	<0.0001
X_2	31.67	1	412.85	<0.0001
X_3	7.64	1	95.43	<0.0001
X_4	0.01	1	0.11	0.4851
X_1^2	0.03	1	0.48	0.2361
X_2^2	1.008	1	9.56	0.00145
X_3^2	0.01	1	0.04	0.2878
X_4^2	13.82	1	114.73	<0.0001
X_1X_2	0.003	1	0.47	0.2539
Model	514.78	9	542.56	<0.0001
Total	516.46	28		

The model's validity is approved by fitting, calculated values (C_{cal}) against obtained (C_{exp}) of the output concentration of mercaptan (Fig 14).

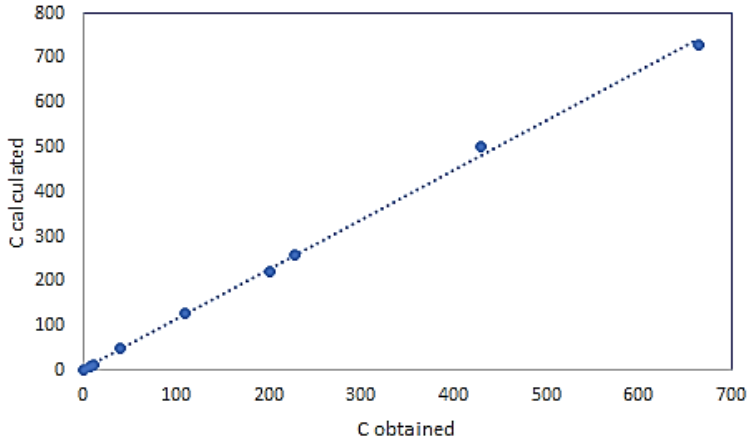

Fig 14. calculated vs. obtained amount of output concentration of mercaptan

The results on Fig. 14 confirmed that the data are not separating very much from the straight-line which income that the calculated data fits very well with the obtained results of mercaptan desulfurization experiments.

Conclusion

The nanostructure graphitic carbon nitride (g-C3N4) with specific area about 432.4 m^2/g was synthesized with new method at 380 0C under the atmospheric air. The high pore volume, large specific area, small pore size and high sorption capacity, made GCN defined from the other synthesized carbon nitrides. TEM and SEM images verified that the structure is porous and the size of the synthesized GCN sheets are about 30 nm. Due to the nano sized structure of the GCN, the surface area and therefore adsorption capacity increased versus to the other synthesized carbon nitride. The removal efficiency of the DBT adsorption of the GCN is about 80% and the adsorption capacity was calculated to be 39.1 mg/g at 25 0C, with 3 g of loaded adsorbent for 600 min from the liquid stream. The equilibrium studies proved that the Freundlich model fitted the data which observed as a physical adsorption process. Pseudo second order model was in good agreement with kinetics data. Due to the negative value of the ΔG^0 and ΔH^0, an exothermic adsorption process was determined. The adsorptive desulfurization process was completed by two types of mercaptans (DBT, TBM). The adsorption capacity of DBT and TBM was calculated as 39.1 and 25.8 mg/g respectively. Due to the formation of N–C bonds over the GCN samples and observation of π–π interactions with the DBT molecules, the removal efficiency of the DBT (80%) as an adsorbate was more increased than TBM (67%) as a liner adsorbate. In addition, the mercaptan removal efficiency of pristine CNT and synthesized GCN exposed the importance of the surface chemical property's role in mercaptan adsorption process.

GRANT SUPPORT DETAILS

The present research did not receive any financial support.

CONFLICT OF INTEREST

The authors declare that there is not any conflict of interests regarding the publication of this manuscript. In addition, the ethical issues, including plagiarism, informed consent, misconduct, data fabrication and/ or falsification, double publication and/or submission, and redundancy has been completely observed by the authors.

LIFE SCIENCE REPORTING

No life science threat was practiced in this research.

REFERENCES

Khan, N. A., Hasan, Z. and Jhung, S. H. (2013). Adsorptive removal of hazardous materials using metal-organic frameworks (MOFs): A review. J. Hazard. Mat., 2; 444–456. https://doi.org/10.1016/j.jhazmat.2012.11.011

Hoseini, D., Z. and Meshkat, S. S.. (2019). Experimental and modeling study of asphaltene adsorption by carbon nanotubes frommodel oil solution. J. Pet. Sci. Eng. 174; 1053-1061.

Fallah, R. N. and Azizian, S. (2012). Removal of thiophenic compounds from liquid fuel by different modi fi ed activated carbon cloths. Fuel Proc. Tech., 93(1); 45–52. https://doi.org/10.1016/j.fuproc.2011.09.012.

Advances, R. S. C. and Srivastava, V. C. (2012). Advances An evaluation of desulfurization technologies for sulfur removal from liquid fuels. RSC. adv., 2; 759–783. https://doi.org/10.1039/c1ra00309g.

Deliyanni, E., Seredych, M. and Bandosz, T. J. (2009). Interactions of 4 , 6 Dimethyldibenzothiophene with the Surface of Activated Carbons. Langmuir, 25(16); 9302–9312. https://doi.org/10.1021/la900854x.

Kumagai, S., Ishizawa, H. and Toida, Y. (2010). Influence of solvent type on dibenzothiophene adsorption onto activated carbon fiber and granular coconut-shell activated carbon. Fuel. 89(2); 365–371. https://doi.org/10.1016/j.fuel.2009.08.013.

Meshkat, S.S., Tavakoli, O. and Rashidi, A.M. (2018). Removal of mercaptan from natural gas condensate using N-doped carbon nanotube adsorbents: Kinetic and DFT study. J. Nat. Gas. Sci. Eng., 55; 288-297.

Seredych, M. and Bandosz, T. J. (2010). Adsorption of Dibenzothiophenes on Nanoporous Carbons : Identification of Specific Adsorption Sites Governing Capacity and Selectivity. Amer. Chem. Soc.,(34); 3352–3360. https://doi.org/10.1021/ef9015087.

Khaled, M. (2015). Adsorption performance of multiwall carbon nanotubes and graphene oxide for removal of thiophene and dibenzothiophene from model diesel fuel. Res. Chem. Intermed., 41; 9817–9833. https://doi.org/10.1007/s11164-015-1986-5.

Kim, J.H., Ma, X., Zhou, A. and Song, C. (2006). Ultra-deep desulfurization and denitrogenation of diesel fuel by selective adsorption over three different adsorbents: a study on adsorptive selectivity and mechanism. Catal. Today, 111; 74–83.

Peng, S. (2018). Removal of low concentration CH3SH with regenerable Cu-doped mesoporous silica. J. Colloid Int. Sci., 513; 903-911.

Saleh, T. A., Al-hammadi, S. A., Tanimu, A. and Alhooshani, K. (2018). Ultra-deep adsorptive desulfurization of fuels on cobalt and molybdenum nanoparticles loaded on activated carbon derived from waste rubber. J. Colloid And Int. Sci., 513; 779-787. https://doi.org/10.1016/j.jcis.2017.11.076.

Moosavi, E. S., Dastgheib, S. A. and Karimzadeh, R. (2012). Adsorption of Thiophenic Compounds from Model Diesel Fuel, Energies, 5(12); 4233-4250. https://doi.org/10.3390/en5104233.

Yua, G.X., Jin, M. Sun, J., Zhou, X.L., Chen, L.F. and Wang, J.A. (2013). Oxidative modification of rice hull based carbon for dibenzothiophene adsorptive removal. Catal. Today. 12; 31–37.

Muzica, M., Biondaa, K. S., Gomzia, Z., Podolskib, S. and Telenb, S. (2010). Study of diesel fuel desulfurization by adsorption. Chem. Eng. Res. Des., 88; 487–495.

Zheng, Y., Lin, L., Wang, B. and Wang, X. (2015). Graphitic carbon nitride polymers toward sustainable photoredox catalysis. Angew. Chem. Int. Ed., 54; 12868-12884.

Thomas, A., Fischer, Goettmann, A., Antonietti, F. M., Müller, J.O., Schlögl, R. and Carlsson, J.M. (2008). Graphitic carbon nitride materials: variation of structure and morphology and their use as metal-free catalysts. J. Mater. Chem., 18; 4893-4908.

Zhao, H., Tian, C., Sun, H., Xiao, K. and Wong, P. K. (2019). Enhanced adsorption and photocatalytic activities of ultrathin graphitic carbon nitride nanosheets :Kinetics and mechanism. Chem. Eng. J., 381; 122760-122778. https://doi.org/10.1016/j.cej.2019.122760.

Muzic, M., Sertic-Bionda, K. and Gomzi, Z. (2008). Kinetic and Statistical Studies of Adsorptive Desulfurization of Diesel Fuel on Commercial Activated Carbons Chem. Eng. Technol., 31; 355-367.

Cao,S., Low, J., Yu, J. and Jaroniec, M. (2015). Polymeric photocatalysts based on graphitic carbon nitride. Adv. Mater., 27; 2150-2176.

Cai, X., He, J., Chen, L., Chen, K., Li, Y., Zhang, K., Jin, Z., Liu, J., Wang, C., Wang, X., Kong, L. and Liu, J. (2017). A 2D-g-C3N4 nanosheet as an eco-friendly adsorbent for various environmental pollutants in water. Chemosphere 171; 192-201.

Hu, R., Wang, X., Dai, S., Shao, D., Hayat, T. and Alsaedi, A. (2015). Application of graphitic carbon nitride for the removal of Pb (II) and aniline from aqueous solutions. Chem. Eng. J., 260; 469–477.

Gao, G., Jiao, Y., Waclawik, E. R. and Du, A. (2016). Single Atom (Pd / Pt) Supported on Graphitic Carbon Nitride as an E ffi cient Photocatalyst for Visible-Light Reduction of Carbon Dioxide. J. Am. Chem. Soc., 138(19); 6292–6297 https://doi.org/10.1021/jacs.6b02692.

Jha, D., Mubarak, N. M., Belal, M., Kumar, R. and Balathanigaimani, M. S. (2019). Adsorptive removal of dibenzothiophene from diesel fuel using microwave synthesized carbon nanomaterials. Fuel, 244; 132–139.

Mguni, L. L., Yao, Y., Nkomzwayo, T., Liu, X. and Glasser, D. (2018). Desulphurization of diesel fuels using intermediate Lewis acids loaded on activated charcoal and alumina activated charcoal and alumina. Chem. Eng. Communi., 0 (0); 1–9. https://doi.org/10.1080/00986445.2018.1511983.

Xu, X., Zhang, S., Li, P. and Shen, Y. (2013). Equilibrium and kinetics of Jet-A fuel desulfurization by selective adsorption at room temperatures. Fuel, 111; 172–179. https://doi.org/10.1016/j.fuel.2013.04.068.

Tang, N., Niu, C., Li, X., Liang, C., Guo, H., Lin, L. and Zeng, G. (2018). Science of the Total Environment Ef fi cient removal of Cd 2 + and Pb $^{2+}$ from aqueous solution with amino- and thiol-functionalized activated carbon: Isotherm and kinetics modeling. Sci. Total Envir., 635; 1331–1344.

Earvin, A., Choi, S., Roces, S., Dugos, N. and Wan, M. (2017). Adsorption of benzothiophene sulfone over clay mineral adsorbents in the frame of oxidative desulfurization. Fuel. 205; 153–160.

Habimana, F., Huo, Y., Jiang, S. and Ji, S. (2016). Synthesis of europium metal – organic framework (Eu-MOF) and its performance in adsorptive desulfurization. Adsorption, 1244; 1147–1155. https://doi.org/10.1007/s10450-016-9838-1.

Batten, S.R., Champness, N.R. and Chen, X.M. (2013). Terminology of metal–organic frameworks and coordination polymers (IUPAC Recommendations. Pure Appl. Chem. 85; 1715–1724.

Lin, Z.J., Yang, Z., Liu, T.F., Huang, Y.B. and Cao, R. (2012). Microwave-assisted synthesis of a series of lanthanide metal–organic frameworks and gas sorption properties. Inorg. Chem., 51; 1813–1820.

Sano, Y., Sugahara, K., Choi, K.H., Korai, Y. and Mochida, I. (2005). Two-step adsorption process for deep desulfurization of diesel oil. Fuel, 84; 903–910.

JabariSeresht, R., Jahanshahi, M., Rashidi, A. M. and Ghoreyshi, A. A. (2013). Synthesize and characterization of graphene nanosheets with high surface area and nanoporous structure. Appl. Surf. Sci., 276; 672–681.

Díaz-Díez, M. A., Gómez-Serrano, V., Fernández-González, C., Cuerda-Correa, E. M. and Macías-García, A. (2005). Porous texture of activated carbons prepared by phosphoric acid activation of woods. Appl. Surf. Sci., 238; 309–313.

Szabo, T., Berkesi, O. and Dekany, I. (2005). Drift study of deuterium-exchanged graphite oxide. Carbon, 43; 3186–3189.

Zhao, D., Sun, Z., Li, F., Liu, R. and Shan, H. (2008). Oxidative desulfurization of thiophene catalyzed by (C4H9)4NBr·2C6H11NO coordinated ionic liquid. Energy Fuels, 22; 3065–3069.

Kwon, T., Nishihara, H., Itoi, H., Yang, Q-H. and Kyotani, T. (2009). Enhancement mechanism of electrochemical capacitance in nitrogen-/boron-doped carbons with uniform straight nanochannels. Langmuir, 25(19); 11961-11968.